International Journal of Heat and Mass Transfer 52 (2009) 2516–2527

Contents lists available at ScienceDirect

International Journal of Heat and Mass Transfer

journal homepage: www.elsevier.com/locate/ijhmt

Prediction of thermal conductivity of nanostructures: Influence of phonon dispersion approximation

D. Baillis *, J. Randrianalisoa

CETHIL UMR5008, CNRS, INSA-Lyon, Université Lyon 1, F-69621 Villeurbanne, France

ARTICLE INFO

Article history:
Received 5 February 2008
Received in revised form 5 January 2009
Available online 28 February 2009

ABSTRACT

In this study, the influence of phonon dispersion approximation on the prediction of in-plane and out-of-plane thermal conductivity of thin films and nanowires is shown. Results obtained using the famous Holland dispersion approximation and the Brillouin zone boundary condition (BZBC) dispersion curves are compared. For (in-plane and out-of-plane) thermal conductivity predictions based on BZBC dispersion curves, new relaxation time parameters fitted from experimental data of bulk silicon thermal conductivity are reported. The in-plane thermal conductivity of nanostructures (films of thicknesses 20 nm, 100 nm, and 420 nm and nanowires of widths 22 nm, 37 nm, and 100 nm) in the temperature range 20–1000 K is calculated from the modified bulk thermal conductivity model by scaling the bulk phonon mean free path (MFP) by the Fuch–Sondheimer factor of boundary scattering developed for nanostructures with rectangular cross-section. The pseudo out-of-plane thermal conductivity of films of thicknesses 20 nm, 100 nm, and 420 nm and in the temperature range 150–1000 K is calculated from the solution of the Boltzmann transport equation (BTE) for phonons by using the Discrete ordinate method (DOM), and the Monte Carlo (MC) simulation. In order to confirm the current results, the calculated in-plane thermal conductivity of silicon thin films and silicon nanowires are compared with existing experimental data. Moreover, due to lack of experimental and theoretical data of out-of-plane thermal conductivity of thin films, comparison of the DOM and MC simulation is performed. The current work shows that a drastic simplification of dispersion curves can lead to wrong prediction of both in-plane and out-of-plane thermal conductivities of nanostructures, especially for ultra thin nanostructures and/or at high temperatures. Comparison with experimental data of in-plane thermal conductivity of silicon thin films and silicon nanowires proves that more refined dispersion approximation such as the BZBC is well adequate for phonon transport calculations when confinement has negligible effect. Moreover, the comparison between the thermal conductivity in the out-of-plane direction and that in the in-plane direction enables one to quantify the anisotropy of thermal conductivity of the film.

1. Introduction

Heat conduction in dielectric and semiconductor nanostructures is a critical issue in the design of electronic devices and packages. Depending on material properties, when the material size is comparable or smaller than the Mean free path (MFP) of phonons, the usual macroscale heat conduction equation known as Fourier law is questionable. In this case, the heat transport can be well modeled by the Boltzmann transport equation (BTE) for phonons [1] and the Molecular dynamics (MD) simulation [2–5]. Particularly, the study of in-plane thermal conductivity of thin films and nanowires, and the out-of-plane thermal conductivity of thin films attracts great interest as it is discussed just below.

The in-plane thermal conductivity of silicon thin films and nanowires has been studied since ten years ago and now, experimental data and predictions results of in-plane thermal conductivity are available. Asheghi and co-workers [6,7] have developed experimental devices based on a Joule heating and electrical-resistance thermometry to measure thermal conductivity along thin films of thicknesses ranging from 20 nm to 3 μm and for temperatures in the range 20–500 K. A similar experimental device has been developed by Li et al. [8] to measure the thermal conductivity along silicon nanowires of width from 22 nm to 115 nm and over the temperature range from 20 K to 320 K. The most useful theoretical model is based on the famous Holland's model of bulk thermal conductivity [9] in which corrections of the bulk phonon relaxation time due to boundary scattering are applied [6,7,10–12]. Other approaches, more complex but more general, have been used to calculate the in-plane conductivity of silicon thin films and nanowires. They consist (i) to solve numerically the BTE for phonons by using either the Structured finite volume method [13], the Discrete ordinate method (DOM) [14], or the Lattice Boltzmann method [15]; (ii) to simulate stochastically phonon transport using

* Corresponding author.
E-mail address: dominique.baillis@insa-lyon.fr (D. Baillis).

0017-9310/$ - see front matter © 2009 Elsevier Ltd. All rights reserved.
doi:10.1016/j.ijheatmasstransfer.2009.01.017

Nomenclature

a	lattice parameter, m
B	relaxation time parameter
C	phonon heat capacity, J K^{-1}
$\mathscr{D}$	phonon density of states per unit volume, m^{-3}
d	distance, m
d_0	sample characteristic size in Eq. (14), m
$d\Omega$	elementary solid angle, sr
F	scaling factor of the intrinsic mean free path due to boundary scattering or Fuch–Sondheimer factor
F_0, F_B	constants in Eqs. (14) and (25), respectively
f	fractional concentration of species in Eq. (16)
G	reciprocal lattice wave vector, m^{-1}
h	height of the cross-section S, m
$\hbar$	Planck's constant divided by 2π, Js rad^{-1}
I	phonon intensity, W m^{-1} sr^{-1}
K	number of bands to discretize the frequency space
k	thermal conductivity, W m^{-1} K^{-1}
k_B	Boltzmann's constant, J K^{-1}
Kn	Knudsen number
L	path length in Eqs. (25) and (26)
ℓ	dimension of film in the out-of-plane direction, m
M	atomic mass, kg
N	number of directions of Gaussian quadrature
p	specular probability parameter
Q	heat or phonon flux, W
q	heat flux per unit surface, W m^{-2}
S	sample cross-section, m^2
T	temperature, K
V_i, V_0	volume of the cell i, average volume, respectively, m^3
v_s, v_g, v_p	average velocity, group velocity, phase velocity, respectively, m s^{-1}
w	width of the cross-section S, m, or angular weight of Gaussian quadrature

Greek symbols

Δ	vector characterizing the phonon direction
Φ	scattering phase function
η	surface roughness of nanostructures, m
κ	wave number or wave vector, m^{-1}
Λ	mean free path, m
λ	wavelength, m
μ	cosine of the angle between the phonon direction and the out-of-plane direction of nanostructure
Θ	angle between the phonon direction and the in-plane direction of nanostructure, rad
θ	polar angle, rad
σ	scattering coefficient, m^{-1}
τ	relaxation time, s
ω	angular frequency, rad s^{-1}
ξ	random number uniformly distributed between 0 and 1

Subscripts

B	boundary scattering or BZBC dispersion model
H	Holland dispersion approximation
I	impurity scattering
in	in-plane thermal conductivity
int	intrinsic scattering in bulk material
ℓ	boundary at the abscise $y = \ell$
m	value of frequency or wave number at the boundary of the first Brillouin zone
min, max	lower and upper limit of the Fuch-Sondheimer factor F
N	normal process
new	new point of phonon interaction
out	out-of-plane thermal conductivity
sc	corrected mean free path or relaxation time due to boundary scattering
0	low frequency phonons or boundary at the abscise $y = 0$
1/2	frequency at wave number at the middle of the first Brillouin zone
3ph	three-phonon scattering process

Superscripts

0	equilibrium intensity
*	dimensionless quantity
+	phonons emitted from an element
−	phonons absorbed at an element

the MC simulation [16–19]; or (iii) to solve the atom motion equations using the MD simulation [2,4,5].

While the thermal conductivity measurement in the in-plane direction of thin films has been carried out successfully, that in the out-of-plane direction of thin films still not performed, may be due to experimental challenges. Therefore, the modeling appears the most suitable approach to determine the out-of-plane thermal conductivity of nanostructures. Nevertheless, the calculations of out-of-plane thermal conductivity of nanostructures are rare in literature. The reported data are mainly obtained from the MD simulation [3–5].

In previous calculations of in-plane thermal conductivity of nanostructures, various phonon dispersion models have been usually used with the Holland's phonon relaxation times. However, the boundary scattering parameter has been often adjusted so that a globally good agreement between the calculations and measurements was noted. For example, for the identical silicon thin films mentioned just above, specular reflection probability at boundaries, namely p, equal to 0, 0.4, and 0.6 have been considered in references [7,19,13,16,17], respectively.

Usually, theoretical approaches except for the MD simulation use phonon dispersion curves and relaxation times as input data. Concerning the phonon dispersion curves, the Holland's approximation [6,7,10] and more refined approximations based on experimental data [16,17,20] such as the Brillouin zone boundary condition (BZBC) model are the most adopted. The relaxation time formulations suggested by Holland have been usually considered for crystalline materials such as silicon and germanium. These recent years, investigations have pointed out the influence of phonon dispersion approximation on the thermal conductivity prediction. Chung et al. [20] compared the calculated bulk thermal conductivities of germanium obtained from different dispersion curve approximations while considering the Holland's formulations of relaxation times. They showed that for each phonon dispersion model, the parameters of Holland's relaxation times should be corrected to predict accurately the bulk thermal conductivity. Mingo et al. calculated the in-plane thermal conductivity of silicon and germanium nanowires using the so-called "atomistic model" that uses the nanowire dispersion relations [21]. Their results have been compared against experimental data of silicon nanowires of different widths [8]. Moreover, calculation based on the famous Callaway model of thermal conductivity that uses a single and effective linear dispersion relation [9] and the Holland model of thermal conductivity that separates the contribution of longitudinal and transverse phonon modes and semi-linear dispersion curves [9] are also reported in Mingo et al. works. It was noted

by these authors that the calculations based on the Callaway and Holland thermal conductivity models could unable to predict thermal conductivity of nanowires without adjusting the phonon dispersion and relaxation time parameters from thermal conductivity measurements of nanowires.

The modification of acoustic phonon spectrum, in ultra-thin free-standing films or nanowires can lead to changes in the phonon group velocity, density of states, and phonon relaxation rates. This effect is called phonon confinement. It has been shown in reference [21] that for thin films and nanowire of characteristic size greater than 20–30 nm the confinement has negligible effect on the heat transport. Indeed a good agreement between calculation from phonon dispersion of bulk material and from phonon dispersion of nanostructure accounting for phonon confinement can be observed in these cases. For engineering computations and when the modification of phonon dispersion curves due to confinement has negligible effect on the heat transport (as it is generally the case in thin films and nanowires of characteristic size greater than 20–30 nm [21]), it is clear that the heat transfer models based on phonon dispersion curves and relaxation times of bulk material are more straightforward than the atomistic model [21] and the MD simulations. Therefore, in the limit of negligible confinement effect, the questions are: can calculations based on bulk phonon dispersion and relaxation times be predictive (i.e. can they predict thermal conductivity of nanostructures without fitting the dispersion curves and the relaxation times parameters from thermal conductivity measurement of these nanostructures)? What are the deviations between thermal conductivity of nanostructured materials using different bulk phonon dispersion approximations? What bulk phonon dispersion approximation is more appropriate? Are the same conclusions valid for in-plane and out-of-plane thermal conductivity calculations?

The main objective of this paper is to answer to the above questions. Moreover, it completes previous ones of Chung et al. [20] and Mingo et al. [21]. Recall that Chung et al. have studied the bulk thermal conductivity and Mingo et al. are interested on thermal conductivity of nanowires using the atomistic model. The current study investigates the influence of phonon dispersion approximation on thermal conductivity of silicon thin films in both in-plane and out-of-plane directions, and that in nanowire longitudinal direction. For in-plane thermal conductivity, we use a model of in-plane thermal conductivity for nanostructures with rectangular cross-section. The calculation results are compared with experimental data of silicon thin films and silicon nanowires reported earlier. Moreover, we propose to calculate the out-of-plane thermal conductivity of thin films using the DOM and MC simulation. In both methods, we account for the non-linearity of phonon dispersion, transverse and longitudinal polarization modes, and the phonon relaxation times dependent on frequency, polarization and temperature. Due to lack of experimental data of out-of-plane thermal conductivity, we compare the results from the DOM and MC simulation each other. The comparison of DOM and MC simulation on the out-of-plane thermal conductivity is an original contribution of the current work. Moreover, a comparison between the in-plane and out-of-plane thermal conductivities of silicon films enables to investigate the thermal conductivity anisotropy.

The paper is organized as follow: at first, the bulk thermal conductivity model, the Holland and BZBC approximations of phonon dispersion, and the formulations of phonon relaxation times are recalled. Then, the in-plane thermal conductivity model of nanostructures with rectangular cross-section (suitable for both thin films and nanowires) is described. The DOM and MC method to calculate the out-of-plane thermal conductivity of thin films are presented. Finally, the results of thermal conductivity in the in-plane and out-of-plane direction of silicon thin films are discussed.

1.1. Bulk thermal conductivity

The bulk thermal conductivity, assuming an isotropic crystal and neglecting the contributions of optical phonons, has been predicted to be of the form [9]:

$$k = k_T + k_L \tag{1}$$

The first term on the right hand side of Eq. (1) corresponds to the contribution of transverse acoustic phonon modes (indexed by "*T*") while the second one corresponds to the contribution of longitudinal acoustic phonon mode (indexed by "*L*"). For bulk crystal k_T and k_L can be expressed as [9,20]:

$$k_T = \frac{2}{3}\int_0^{\omega_{m,T}} C_T(\omega)\, v_{g,T}^2(\omega)\tau_T(\omega,T)\, d\omega \tag{2}$$

$$k_L = \frac{1}{3}\int_0^{\omega_{m,L}} C_L(\omega)\, v_{g,L}^2(\omega)\tau_L(\omega,T)\, d\omega \tag{3}$$

where ω is the angular frequency. $\omega_{m,T}$ and $\omega_{m,L}$ are the upper limits of the angular frequencies of transverse and longitudinal phonon branches, respectively. τ_T and τ_L are the respective transverse and longitudinal effective phonon relaxation times of phonons in the crystal. $v_{g,T}$ and $v_{g,L}$ are the phonon group velocities of transverse and longitudinal modes, respectively. C_j is the heat capacity per normal mode of frequency ω and polarization $j = T, L$ at temperature T, defined by:

$$C_j = \frac{x^2 k_B e^x \mathscr{D}_j(\omega)}{(e^x-1)^2} \qquad \text{for } j = T, L \tag{4}$$

where $x = \hbar\omega/k_B T$, $k_B = 1.38 \times 10^{-23}$ J/K is the Boltzmann's constant, and $\hbar = 1.054 \times 10^{-34}$ Js/rad is the Planck's constant divided by 2π. D_j is a density of states (DOS) per unit volume of phonons of frequency ω and polarization mode $j = T, L$ such as [20,22]:

$$\mathscr{D}_j(\omega) = \frac{\kappa^2}{2\pi^2 v_{g,j}} = \frac{\omega^2}{2\pi^2 v_{g,j} v_{p,j}^2} \qquad \text{for } j = T, L \tag{5}$$

The phonon group velocity, v_g, is defined as $\partial\omega/\partial\kappa$ where κ is the wave number. The phonon phase velocity, v_p, is defined as ω/κ.

When the scattering processes are independent, the effective scattering relaxation times are additive according to the Mathiensen rule [9]:

$$\tau_j^{-1} = \tau_{B,j}^{-1} + \tau_{I,j}^{-1} + \tau_{3ph,j}^{-1} \qquad \text{for } j = T, L \tag{6}$$

where τ_B, τ_I, and τ_{3ph} are the usual boundary, impurity or defect, and three-phonon relaxation times, respectively.

1.1.1. Phonon dispersion in silicon

Silicon is probably the most important electronic material to date. Several researchers have performed studies of silicon in the past, and as a result, its phonon dispersion characteristics are well known. Experimental data of phonon dispersion of the acoustic modes in the [1 0 0] crystal direction of silicon at room temperature [23] are shown in Fig. 1. The horizontal axis is a dimensionless wave number $\kappa^* = \kappa/\kappa_m$ where $\kappa_m = 2\pi/a$ the wave number at the edge of the first Brillouin zone [22,24], with $a = 0.543$ nm the silicon lattice size parameter. The upper limits of the angular frequencies of the phonon branches obtained from experimental data are [22,23]:

$$\omega_{m,T} = 210 k_B/\hbar \text{ rad/s} \tag{7}$$

$$\omega_{m,L} = 570 k_B/\hbar \text{ rad/s} \tag{8}$$

In calculations of thermal properties (such as thermal conductivity and heat capacity), phonon dispersion curves are required. Moreover, it is usually assumed that the first Brillouin zone is iso-

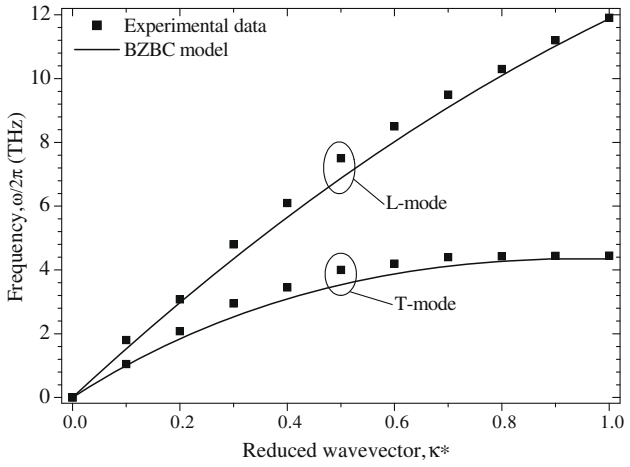

Fig. 1. Silicon dispersion curves of acoustic phonons in the [001] crystal direction. Solid symbols: experimental data [23]; solid lines: BZBC models.

tropic, which means that the dispersion curves are identical in any wave vector direction. They are usually taken equal to that in the [100] wave vector direction.

1.1.1.1. Holland approximation. The most simple model that accounts for the non-linearity of phonon dispersion and the different polarization branches is the Holland's model [9]. Holland separated the contributions of *T* and *L* phonons modes, and includes a partial effect of non-linear phonon dispersion by splitting each polarization branch into two regions at the middle of the first Brillouin zone, i.e. at $\kappa^* = 0.5$. Indeed, for each polarization mode $j = T, L$, the first region corresponds to frequencies and wave numbers in the ranges $0 \leqslant \omega < \omega_{1/2,j}$ and $0 \leqslant \kappa^* < 0.5$, respectively, while the second one corresponds to frequencies and wave numbers in the ranges $\omega_{1/2,j} \leqslant \omega \leqslant \omega_j$ and $0.5 \leqslant \kappa^* \leqslant 1$, respectively, where $\omega_{1/2,T} = 2.47 \times 10^{-13}$ rad/s and $\omega_{1/2,L} = 4.58 \times 10^{-13}$ rad/s are experimentally data of angular frequencies corresponding to $\kappa^* = 0.5$ [23].

The Holland dispersion approximation assumed that "the group velocity and phase velocity are constant at each region and for each polarization mode", i.e.:

For $0 \leqslant \omega < \omega_{1/2,j}$:

$$v_{g,j} = v_{0,j} = \begin{cases} 5860 \text{ m/s} & \text{for} \quad j = T \\ 8480 \text{ m/s} & \text{for} \quad j = L \end{cases} \tag{9}$$

For $\omega_{1/2,j} \leqslant \omega \leqslant \omega_j$:

$$v_{g,j} = \begin{cases} 2000 \text{ m/s} & \text{for} \quad j = T \\ 4240 \text{ m/s} & \text{for} \quad j = L \end{cases} \tag{10}$$

1.1.1.2. The Brillouin zone boundary condition (BZBC) model. In order to better reproduce the experimental phonon dispersion, polynomial functions are usually used. The BZBC model introduced by Chung et al. [20] uses low order polynomial; thus, it is chosen in this study. A quadratic wave number dependence for *L*-phonons and a cubic wave number dependence for *T*-phonons are used and both satisfy the first Brillouin zone boundary conditions such as:

$$\begin{cases} \kappa_j = 0 \quad \text{for } \omega = 0 \\ \partial\kappa_j/\partial\omega = 1/v_{g,j} = 0 \quad \text{for } \omega = 0 \quad j = T, L \\ \omega = \omega_{m,j} \quad \text{for } \kappa = \kappa_m \end{cases} \tag{11}$$

The BZBC phonon dispersion relations as function of the reduced wave number are:

For longitudinal (*L*) phonon branch:

$$\omega = v_{0,L}\kappa_m\kappa^* + (\omega_L - v_{0,L}\kappa_m\kappa^*)^2 \tag{12}$$

For transverse (*T*) phonon branches:

$$\omega = v_{0,T}\kappa_m\kappa^* + (3\omega_T - 2v_{0,T}\kappa_m)\kappa^{*2} + (v_{0,T} - 2\omega_T)\kappa^{*3} \tag{13}$$

The phonon dispersion curves deduced from BZBC model [Eqs. (12) and (13)] are also showed in Fig. 1. It can be seen that BZBC curves match reasonably well experimental data overall the first Brillouin zone.

1.1.2. Scattering relaxation times

1.1.2.1. Boundary scattering. Boundary scattering refers to scattering of phonons with material boundaries. The phonon relaxation time due to the boundary scattering in bulk material can be given by [9]:

$$\tau_{B,j}^{-1}(\omega) = \frac{v_{g,j}(\omega)}{F_0 d_0} \qquad \text{for } j = T, L \tag{14}$$

where F_0 is a constant that account for both the finite length to thickness ratio and the smoothness of the surface. $d_0 = 2\sqrt{S/\pi}$ is the sample characteristic size of cross-section area *S*.

1.1.2.2. Impurity scattering. The heat transport is sensitive to defects and impurities, which include the isotopic content of an otherwise pure crystal. The phonon wavelengths are larger than the impurities typical size. Indeed the typical phonon wavelength are in the nm range whereas the defects are in the angström range. The Rayleigh regime is then applicable. Therefore, the scattering time is inversely proportional to the frequency^4. The impurity (or defect) relaxation time can be expressed as follow in according to the Rayleigh regime in the radiation theory [9]:

$$\tau_{I,j}^{-1} = B_{I,j}(\omega)\,\omega^4 \qquad \text{for } j = T, L \tag{15}$$

with:

$$B_{I,j}(\omega) = V_0 \frac{\sum_i f_i[1 - (M_i/M)]^2}{4\pi v_{g,j}(\omega) v_{p,j}^2(\omega)} \qquad \text{for } j = T, L \tag{16}$$

where V_0 is the average volume of a unit cell, f_i is the fractional concentration of species *i*, M_i is the atomic mass of species *i* of average atomic mass *M*.

1.1.2.3. Three phonon scattering. At temperature smaller than the Debye temperature, the main types of phonon–phonon scattering are the three-phonon processes. They include the reversible Normal process, referred to *N*, characterized by the momentum conservation $\kappa_1 + \kappa_2 \leftrightarrow \kappa_3$ and Umklapp process, referred to *U*, and characterized by the relation $\kappa_1 + \kappa_2 \leftrightarrow \kappa_3 + G$. κ_1, κ_2, and κ_3 are the wave vectors of phonons undergoing to the process and *G* is a reciprocal lattice wave vector [22,24]. Note that both processes conserve energy during the collision.

The study of three-phonon scattering has attracted much attention and several more or less complex formulations are suggested [9,25,26]. Nevertheless, in each case, there is at least one unknown parameter that requires fitting from mechanical and/or thermophysical property measurements. Holland [9] summarized the most useful formulations where the contributions of longitudinal (*L*) and transverse acoustic phonons (*T*) are separated so that a relaxation time is associated with each phonon polarization mode.

From Holland paper [9], the usual *N* and *U* relaxation times for the transverse and longitudinal polarization modes are:

$$\tau_{3ph,L}^{-1} = \tau_{N,L}^{-1} + \tau_{U,L}^{-1} = B_L\omega^2T^3 \qquad \text{for } N \text{ and } U \text{ processes} \tag{17}$$

$$\tau_{3ph,T}^{-1} = \tau_{N,T}^{-1} + \tau_{U,T}^{-1} \qquad \text{for } N \text{ and } U \text{ processes} \tag{18}$$

with:

$$\tau_{N,T}^{-1}(\omega,T)=\begin{cases}B_{N,T}\omega T^4, & \text{for} \quad \omega<\omega_{1/2,T}\\ 0, & \text{for} \quad \omega>\omega_{1/2,T}\end{cases} \text{ for } N \text{ process} \tag{19}$$

$$\tau_{U,T}^{-1}(\omega,T)=\begin{cases}0, & \text{for} \quad \omega<\omega_{1/2,T}\\ B_{U,T}\frac{\omega^2}{\sinh(\hbar\omega/k_BT)} & \text{for} \quad \omega>\omega_{1/2,T}\end{cases} \text{ for } U \text{ process} \tag{20}$$

B_I, B_L, $B_{N,T}$, and $B_{U,T}$ are the called relaxation time parameters. In practice, they, as well as, the factor F_0 in Eq. (14), are determined from a fit between theoretical and experimental thermal conductivities of bulk material over a wide temperature range [20]. Therefore, their values depend on the model accuracy, especially on the phonon dispersion model as it has been shown for germanium [20]. In this study, in each dispersion approximation, the relaxation time parameters are adjusted only from bulk thermal conductivity measurement using Eqs. (1)–(3). According to Eq. (16), the impurity parameter B_I is inversely proportional to the velocity product $v_g v_p^2$ but in the Holland dispersion approximation, B_I is inversely proportional to v_s^3 (where v_s is an average velocity of longitudinal and transverse branches at low frequencies). In the BZBC dispersion model, a more refined consideration of B_I is performed. This consists to separate the cases of longitudinal and transverse modes, and the cases of low and high frequencies. The usual Holland relaxation time parameters and the new relaxation time parameters associated to the BZBC dispersion model are summarized in Tables 1 and 2, respectively. Note that in the atomistically approach suggested by Mingo et al. [21], the parameters of relaxation times are also adjusted from bulk thermal conductivity data.

1.2. In-plane thermal conductivity of thin films and nanowires

1.2.1. Models of in-plane thermal conductivity

1.2.1.1. Literature review. This last decade, the theoretical study of in-plane thermal conductivity of silicon films and silicon nanowires has attracted great attention thanks to the thermal conductivity measurements carried out by Asheghi and co-workers [6,7] for silicon thin films and Li et al. [8] for silicon nanowires.

The most useful model is based on the bulk thermal conductivity formulation [Eqs. (1)–(3)] in which the bulk phonon relaxation time τ [Eqs. (2) and (3)] is substituted by a corrected relaxation time, τ_{sc}:

Table 1
Holland's relaxation time parameters [9].

Scattering process	Relaxation time parameters		
Boundary	$d_0 = 0.716$ cm; $F_0 = 0.8$; and $v_s = 6400$ m/s		
Impurities or defects	$B_I = 1.32\times10^{-45}$ s^{-3}		
Three-phonon	$B_L = 2\times10^{-24}$ s K^{-3}	$B_{N,T} = 9.3\times10^{-13}$ K^{-3}	$B_{U,T} = 5.5\times10^{-18}$ s

Table 2
Fitted relaxation time parameters using BZBC dispersion model.

Scattering process	Relaxation time parameters	
Boundary	$d_0 = 0.716$ cm, $F_0 = 0.8$	
Impurities or defects	$B_{I,j}(\omega<\omega_{1/2,LorT}) = 1.32\times10^{-45}$ s^{-3}	$B_{I,L}(\omega>\omega_{1/2,L}) = 6.22\times10^{-46}$ s^{-3} $B_{I,T}(\omega>\omega_{1/2,T}) = 2.64\times10^{-46}$ s^{-3}
Three-phonon	$B_L(\omega<\omega_{1/2,L}) = 2.0\times10^{-24}$ s K^{-3} $B_L(\omega\geqslant\omega_{1/2,L}) = 9.4\times10^{-25}$ s K^{-3}	$B_{N,T}(\omega\leqslant\omega_{1/2,T}) = 9.3\times10^{-13}$ K^{-3} and 0 elsewhere $B_{U,T}(\omega>\omega_{1/2,T}) = 1.1\times10^{-18}$ s and 0 elsewhere

$$k_{in}=\frac{1}{3}\sum_{j=L,T,T}\int_0^{\omega_{mj}} C_j(\omega)v_{g,j}^2(\omega)\tau_{sc,j}(\omega,T)\,d\omega \tag{21}$$

(*m*1) Prior works on electrical resistivity of metal films have shown that the ratio between the carrier mean free path in thin metal film and that in bulk metal can be given by the following equation known as Fuch–Sondheimer factor F [27].

$$F(p,\Lambda_{\text{int}},d^*)=1-\frac{3}{2d^*}(1-p)\int_1^{+\infty}\left(\frac{1}{t^3}-\frac{1}{t^5}\right)\frac{1-\exp(td^*)}{1-p\exp(td^*)}dt \tag{22}$$

where $d^* = w/\Lambda_{\text{int}}$ with w the film thickness, p a probability of specular reflection at boundaries, and Λ_{int} the mean free path in bulk material. This equation is derived from solution of the BTE that models both electron and phonon transport, therefore it is suitable not only for electrons but also for phonons.

To determine the phonon relaxation time in thin films τ_{sc}, Asheghi and co-workers [6,7] have used the famous Fuch–Sondheimer's factor F, i.e. Eq. (22), to scale the intrinsic phonon relaxation time in bulk silicon such as

$$\tau_{sc}=\tau_{\text{int}}\times F \tag{23}$$

and

$$\tau_{\text{int}}^{-1}=\tau_I^{-1}+\tau_{3ph}^{-1} \tag{24}$$

(*m*2) The general form of Eq. (21) that consists performing sum over wave vector space instead of performing integral over frequency has been suggested by Chantrenne et al. [10] to model the in-plane thermal conductivity of silicon films and nanowires. Such sum over the wave vector space could enable to capture the anisotropy of the first Brillouin zone; however, these authors have assumed that the first Brillouin zone is isotropic. In this approach, the phonon relaxation time in nanostructures, τ_{sc}, is governed by Eq. (6) except that the following boundary relaxation time is used instead of the relaxation time given by Eq. (14):

$$\tau_{B,j}^{-1}(\kappa)=\frac{v_g(\kappa,j)}{F_B\times L(\Delta)} \qquad \text{for } j=T,L \tag{25}$$

where κ refers to the wave vector, F_B is a constant fitted from bulk thermal conductivity data, therefore its value depends on phonon dispersion model. $L(\Delta)$ is a path length dependent on the wave vector direction, Δ, according to:

$$L(\Delta)=\frac{w}{\sin\Theta} \tag{26}$$

with Θ the angle between the wave direction Δ and the nanostructure in-plane direction. w the thickness (for films) or the width (for wires).

(*m*3) Using the atomistic model, Mingo et al. [21] have predicted the in-plane thermal conductivity of silicon and germanium nanowires. The Mingo et al.' model is similar to Eq. (21), except that the DOS [Eq. (5)] and the velocities v_p and v_g are evaluated using the dispersion curves of the nanowire instead of that of bulk material as it is the case in the model based on Eq. (21). An expression of the effective phonon relaxation time in nanowire, τ_{sc}, similar to that in bulk material, i.e. given by Eq. (6), is considered with a boundary scattering term given by Eq. (14). In the Mingo et al.' model, the boundary scattering parameter F_0 depends on the nanowire width and surface roughness and it has been determined from electronic microscope analyze with values between 1 and 1.3 for nanowires of width between 37 and 115 nm [21].

(*m*4) The other approaches are based on the solution of the BTE for phonons using the DOM [1,13–15], the MC method [16–19] and MD simulation [2–5]. In these approaches, neither the reduction factor F nor the boundary relaxation time τ_B is required because

they accounted for the boundary scattering in the boundary condition.

Although different approaches have been suggested to model the in-plane thermal conductivity of nanostructures, the most practical one is undoubtedly that governed by Eqs. (21)–(24) especially when the phonon confinement has negligible effect as it is the case in nanowires of width greater than 30 nm and in films of thickness greater than 20 nm. In fact, the model governed by Eqs. (21)–(24) does not require adjusting the boundary scattering parameters (F_B and F_0) such it is the case in the approaches ($m2$) [10] and ($m3$) [21] because the boundary scattering can be globally captured by the scaling factor F. Moreover, it requires considerably less numerical effort and computation time than the DOM, MC technique and MD simulation.

1.2.1.2. Current proposed model. Until now, derivation of the scaling factor F for nanostructures with rectangular cross-section has been made to calculate electrical resistivity of metallic wires [28]. We suggest applying it for in-plane thermal conductivity calculation for both thin films and nanowires.

It consists to bound the value of F as follow:

$$F_{\min}(p,\Lambda_{\text{int}},w,h) \le F \le F_{\max}(p,\Lambda_{\text{int}},w,h) \tag{27}$$

$F_{\min}$ is the solution considering that a specular fraction p is assumed at the first and second reflections on the boundaries and neglecting all subsequent reflections. $F_{\max}$ is the solution considering that a specular fraction p is assumed at the first reflection site and the second reflection is completely diffuse. Indeed, the impact of surface scattering is underestimated in $F_{\min}$ and overestimated in $F_{\max}$. The explicit forms of $F_{\min}$ and $F_{\max}$ are recalled in the appendix [Eqs. (A.1) and (A.2)] and for more details concerning their derivation, the reader is recommended to the original paper [28]. The value of the factor F and the absolute error associated with it can be given by:

$$F(p,\Lambda_{\text{int}},w,h) = \frac{F_{\min}+F_{\max}}{2} \tag{28}$$

and

$$\Delta F(p,\Lambda_{\text{int}},w,h) = F_{\min}-F_{\max} \tag{29}$$

In Eqs. (28) and (29), w and h are the width and height of the nanostructure, respectively. An example of the evolution of the reduction factor F given by Eq. (28) as function of the ratio w/Λ_{int} (where w is the thickness for films and the width for wires) is depicted in Fig. 2 for different values of the ratio of height to width, h/w, of the nanostructure considering $p = 0$ (i.e. diffuse boundary scattering). Also the result from the usual Fuch–Sondheimer formula [Eq. (22)] for $p = 0$ is reported. It can be shown that no effect of boundary scattering can be observed from $w/\Lambda_{\text{int}} > 10$. In the other hand, the boundary scattering reduces 96–99% of the bulk mean free path for $w/\Lambda_{\text{int}} \leqslant 0.01$. As the height to width ratio increases, the reduction factor increases. It converges to the film limit [Eq. (22)] with an error less than 5% from the ratio $h/w \geqslant 100$ for any w/Λ_{int} greater than 0.01. The minimal reduction factor value is reached for square cross-section case.

In Eq. (28), F is function of the specular probability parameter p. The value of p is usually adjusted from experimental data of thermal conductivity of nanostructures. We propose to calculate it as function of the frequency of the incident phonon and the surface roughness according to the radiation theory. In fact, for a phonon of angular frequency ω, incident on a random rough surface of roughness η with an angle θ measured from the normal plane to the surface, the parameter p can be expressed as [24,29]:

$$p(\theta,\omega) = \exp(-16\pi^3\eta^2\cos^2\theta/\lambda^2) \tag{30}$$

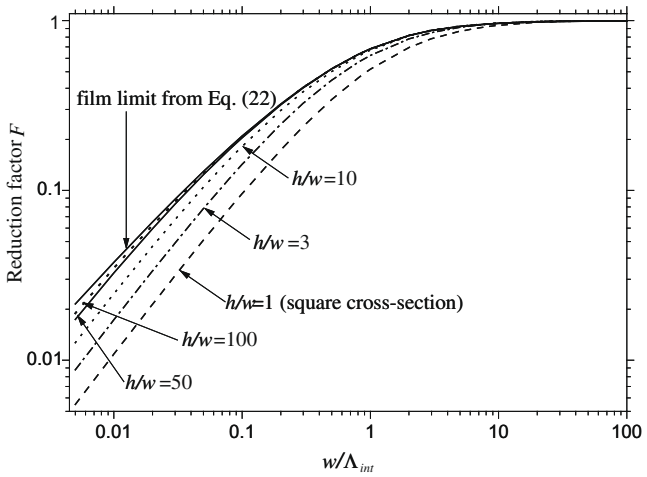

Fig. 2. Reduction factor F as function of the ratio between the nanostructure width and the bulk mean free path for different values of the height to width ratio and for diffuse boundary scattering case ($p = 0$).

with $\lambda = 2\pi v_p/\omega$ the phonon wavelength. It is more useful to use a specular probability parameter independent of the phonon direction θ. A usual averaging over direction of Eq. (30) can be suggested according to radiation theory [30]:

$$p(\omega) = 2\int_0^1 p(\theta,\omega)\mu\,d\mu \tag{31}$$

with $\mu = \cos\theta$.

Generally, the surface roughness of materials is very much greater than phonon wavelength and the boundary scattering is completely diffuse. However, the case of surface roughness comparable to the wavelength may be expected for nanostructures; hence, specular scattering may take place. Let consider the case where the roughness is comparable to the lattice parameter a ($\eta \approx 1.5a$ for example). The evolution of the parameter p given by Eq. (31) as function of the phonon angular frequency in silicon is shown in Fig. 3 for both longitudinal (L-mode) and transverse phonon modes (T-mode). It can be seen that for frequency $\omega > \omega_{1/2,T}$, diffuse scattering takes place else both specular and diffuse reflection prevail.

1.3. Out-of-plane thermal conductivity of thin films

In the case of out-of-plane thermal conductivity of thin films, the heat transport normal to the film interfaces is studied. For heat transport across thin films, the Knudsen number ($Kn = \Lambda_{\text{int}}/\ell$ where ℓ is now the film thickness in the out-of-plane direction of the film) can be much greater or comparable to 1 in which the end effect such as temperature shifts at boundaries may take place and therefore, the thermal conductivity cannot be obtained by Eqs. (1)–(3) or Eq. (21) (since these last equations assume that the length in the heat flux direction is infinite hence there is no temperature shifts at boundaries). It is then necessary to solve the BTE for phonons.

Majumdar [1] has shown that in the microscale regime ($Kn \sim 1$), the heat transport by lattice vibrations or phonons can be analyzed as radiative transfer problem. Based on Boltzmann transport theory, an equation of phonon radiative transfer (EPRT) is developed. For steady-state regime and one-dimensional system, the EPRT can be written as [1]:

$$\mu\frac{\partial I_\omega}{\partial y} = \frac{I_\omega^0 - I_\omega}{\Lambda_{\text{int}}} \tag{32}$$

where μ is the cosine of the angle between the phonon propagation direction and the y direction, which is perpendicular to the film sur-

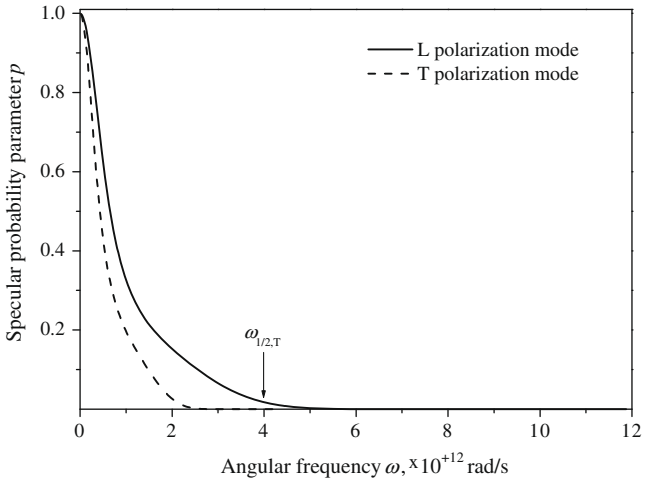

Fig. 3. Evolution of the angular averaged specular probability parameter as function of the angular frequency for $\eta = 1.5a \approx 0.75$ nm with $a = 0.543$ nm.

faces, I_ω is the spectral phonon intensity at the abscise y and propagates along the direction characterized by μ, I^0_ω is the phonon intensity at equilibrium, ω is the frequency, and $\Lambda_{\text{int}} = v_g\tau_{\text{int}}$ is the mean free path between intrinsic scattering in which τ_{int} and v_g are the intrinsic phonon relaxation time given by Eq. (24) and the phonon group velocity, respectively.

With the advent of modern high-speed computers, it is now possible to solve the BTE in its most general form. However, limited progress has been made in the area of solution of the BTE for phonons, i.e. Eq. (32). Works performed by Majumdar [1], Chen and Tien [31], Goodson [32], Chen [33], Pilon and Katika [34] have presented solution strategies but neglecting the non-linear phonon dispersion and the dual polarizations of phonon propagation. In their works, a single average polarization branch is used instead of the dual polarizations of phonons. Recently, more complete analyzes taking into account the non-linear phonon dispersion and the two states of polarization modes were performed by Mazumder and Majumdar using the Monte Carlo method [16] and Narumanchi et al. using Unstructured modified Structured finite volume method [13]. In these cases the Holland's relaxation time formulations and parameters were used.

In the current work, we use the Discrete ordinate method (DOM) to solve the BTE for phonons. Compared to previous works using the DOM, the current one accounts for: (i) the dual polarizations of phonon propagation and non-linear dispersion relationships; (ii) individual treatment of various scattering mechanisms; (iii) the relaxation times dependent on frequency, polarization, and temperature; and (iv) the equilibrium energy condition over all frequencies and polarizations.

As consequence of (i), the case of polarization and frequency dependent EPRT is considered, i.e. the EPRT is solve for each state of polarization [longitudinal (L) and transverse (T)] and for each frequency. Moreover, (ii) implies that the usual EPRT is rewritten to separate the term of scattering by impurities from the term of three-phonon scattering and introducing a scattering phase function and an in-scattering term which makes EPRT exactly same as Equation of radiative transfer (ERT). It can be noted that this formulation of EPRT called generalized EPRT (GEPRT) has been used by Prasher [35] to treat phonon transport in anisotropic scattering particulate media. Recall that for simulation of heat conduction in microscale regime, the non-gray treatment of phonons, i.e. the point (iii), is crucial to obtain realistic results [13]. The last point, i.e. (iv), means that it is possible to have non equilibrium condition at a particular frequency.

Up to date, no experimental data of out-of-plane thermal conductivity of thin films are available, certainly due to the difficulty to perform such experiment with ultra thin films. In this work, we suggest in more the Monte Carlo simulation to compare the results obtained from the DOM. Note that in many cases of transport of particles, the Monte Carlo simulation has been taken usually as method of reference.

1.3.1. Discrete ordinates method (DOM)

1.3.1.1. Governing equations. The generalized EPRT for each polarization state, $j = T,L$ and each frequency, ω, is [35]:

$$\mu\frac{\partial I_{\omega j}}{\partial y} = \sigma_j(I^0_{\omega j} - I_{\omega j}) - \sigma_{Ij}I_{\omega j} + \frac{\sigma_{Ij}}{4\pi}\int_{4\pi}\Phi(\Delta_i,\Delta_j)I_{\omega j}(\Delta_i)d\Omega_i \qquad \text{for } j = T,L \tag{33}$$

where $\sigma_j = 1/(v_{gj}\tau_{3ph,j})$ is called scattering coefficient related to the three-phonon processes, $\sigma_{I,j} = 1/(v_{gj}\tau_{Ij})$ is called scattering coefficient related to the impurity scattering, and $\Phi(\Delta_i, \Delta_j)$ is the phase function defined as the probability for an incident phonon intensity with incident direction Δ_i to be scattered in the direction Δ_j. Note that for isotropic scattering, as it is usually assumed for impurity scattering, $\Phi(\Delta_i, \Delta_j) = 1$. $d\Omega_i$ is an elementary solid angle around the direction Δ_i. $I^0_{\omega j}$ is the equilibrium intensity defined by:

$$I^0_{\omega j} = \frac{1}{4\pi}\frac{v_{gj}\hbar\omega \mathrm{D}_j(\omega)}{\exp(\hbar\omega/k_BT) - 1} \tag{34}$$

In Eq. (34), $D_j(\omega)$ is the DOS given by Eq. (5).

The local heat flux per unit area $q_j(y)$ for each polarization state is related to the intensity field by:

$$q_j(y) = 2\pi\int_0^{\omega_{mj}}\int_{-1}^{1} I_{\omega j}\mu d\mu d\omega \qquad j = T,L \tag{35}$$

where ω_{mj} is the upper limits of the angular frequencies of polarization mode $j = L, T$ given by Eqs. (9) and (10).

The total heat flux per unit area q is the sum of transverse and longitudinal contributions:

$$q = q_L + 2q_T \tag{36}$$

1.3.1.2. Boundary conditions. The boundary conditions are assumed to be perfectly absorbing and emitting isotropically similarly to the photon emission from a black surface [30]:

$$\begin{cases} I_\omega(y=0) = I^0_\omega(T_0) \\ I_\omega(y=\ell) = I^0_\omega(T_\ell) \end{cases} \tag{37}$$

where T_0 and T_ℓ are the prescribed boundary temperatures.

1.3.1.3. Numerical procedure. To carried out frequency integrals in Eqs. (33), (35), and (37), the gray per band approximation is used. It consists to replace the frequency integral into discrete sum of band number with uniform band width $\Delta\omega$. Therefore, for the discrete frequency, ω_k, the scattering coefficients and intensities are assumed to be constant within the spectral band $\Delta\omega$, i.e.:

$$\sigma_\omega = \sigma_k \tag{38}$$

$$I_{kj}(y) = \int_{\omega_{k-1}}^{\omega_k} I_{\omega j}(y)d\omega \text{ and } I^0_{kj}(y) = \int_{\omega_{k-1}}^{\omega_k} I^0_{\omega j}(y)\,d\omega \quad j = T,L \tag{39}$$

The partial derivative in Eq. (33) is treated using control volume method [36] while the angular integrals in Eqs. (33), (35), and (37) are replaced by numerical quadratures [37] of cosine direction μ_n and weight w_n for $n = 1, N$ where N is the direction number. These points constitute the conventional discrete ordinates method.

The solution of GEPRT [Eq. (33)] is then obtained from an iterative method:

(i) For one given temperature field, the intensity for each polarization mode can be calculated at every location, for a set of discrete direction and within each frequency band. Moreover, the phonon fluxes may be evaluated by the following quadrature formula:

$$q_j = 2\pi \sum_{k=1}^{K_j} \sum_{n=1}^{N} w_n I_{k,n,j} \mu_n \qquad j = T, L \tag{40}$$

where K_j is the number of gray bands for the polarization mode j and $I_{k,n,j}$ is the intensity at the frequency band number k, propagating along the direction number n, and of polarization j.

(ii) Knowing phonon intensities and the total phonon heat flux, the steady-state energy balance in the discretized form can be used to retrieve the new temperature field $T(y)$ at every location:

$$2\sum_{k=1}^{K_T} \sigma_{k,T} \left(4\pi I^0_{k,T} - 2\pi \sum_{n=1}^{N} I_{k,n,T} w_n \right) + \sum_{k=1}^{K_L} \sigma_{k,L} \left(4\pi I^0_{k,L} - 2\pi \sum_{n=1}^{N} I_{k,n,L} w_n \right) = 0 \tag{41}$$

(iii) Thus, the main iterative loop within the computation algorithm consists to calculate the intensity fields $I_{k,n,T}$ and $I_{k,n,L}$ for one given temperature field and then updating the temperature field from the energy balance [Eq. (41)] until a convergence criterion on temperature field $T(y)$ is met.

For the spectral discretization, the longitudinal frequency interval $\omega_{m,L}$ is divided into $K_L = 500$ gray bands of uniform band width $\Delta\omega = \omega_{m,L}/K_L$ while the transverse frequency interval $\omega_{m,T}$ is divided into $K_T = K_L\omega_{m,T}/\omega_{m,L}$ gray bands [19]. The spatial domain, i.e. the film thickness, is discretized into 300 regular meshes. The angular space is discretized using the Gaussian quadrature with $N = 24$ directions [38]. The convergence criterion is that the temperature difference between two successive iterations verifies $\Delta T/T < 10^{-4}$ everywhere. Finally, the apparent out-of-plane thermal conductivity of the film, k_{out}, is calculated from the relation:

$$k_{out} = \frac{q}{|\Delta T/\Delta y|} \tag{42}$$

where q is the overall heat flux per unit surface crossing the film. $\Delta T/\Delta y$ is the slope of the temperature field calculated from the first and the last nodes of the spatial mesh nearest from the boundaries. In the semi-ballistic regime, there is temperature shifts at boundaries and in this case $\Delta T/\Delta y$ is the slope of the temperature in the region where temperature profile is linear. It can be noted that k_{out}, defined in Eq. (42), is a pseudo thermal conductivity, and should be used carefully. It is not an intrinsic parameter as it depends on film thickness.

To verify the good behavior of the current DOM, the out-of-plane thermal conductivity of silicon film of thickness $\ell = 100$ μm over a large temperature range ($20\ \mathrm{K} \leqslant T \leqslant 1000\ \mathrm{K}$) is calculated and the result is reported in Fig. 4. It can be shown that for temperature greater than 100 K for which the transport regime is completely diffusive ($Kn < 0.01$), the DOM solution converges well to experimental data of bulk silicon thermal conductivity [9]. Moreover, no effect of dispersion curves model is noted in this temperature range. At low temperature ($T < 100\ K$), the ballistic transport still prevails (Kn is about 0.1 at 60 K and 4–5 at 20 K) leading to temperature shifts at boundaries. Hence, the DOM result deviates from the bulk data.

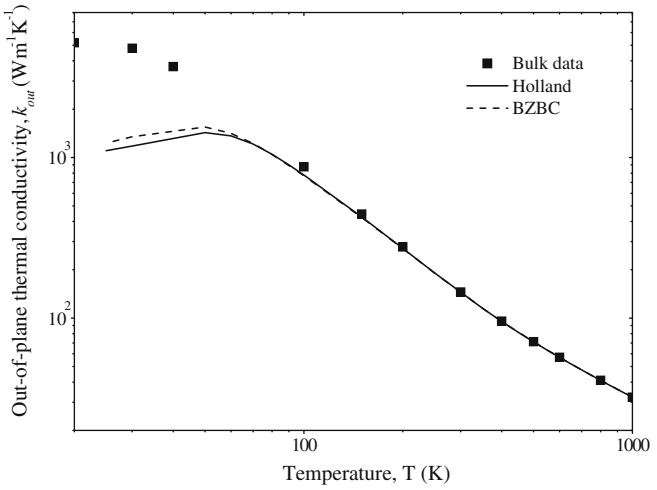

Fig. 4. Comparison of the out-of-plane thermal conductivity of silicon film of thickness 100 μm calculated using the DOM and with experimental data of silicon bulk thermal conductivity [9] over temperature range $20\ \mathrm{K} \leqslant T \leqslant 1000\ \mathrm{K}$.

1.3.2. Monte Carlo simulation

Recently, a MC algorithm to simulate steady-state phonon transport in microscale regime has been developed by the authors [19]. It consists to mimic numerically the guarded hot plate experiment in stationary regime.

The simulation is performed on a 3D box of dimension ℓ in the out-of-plane direction (i.e., in the y axis considered in the DOM) and square cross-section S perpendicular to the y axis. This box is discretized into *Ncell* parallelepiped cells along the y axis. For each cell i is assigned an arbitrary temperature, T_i, which stills to be determined. The size of cells is chosen to be smaller than the intrinsic phonon MFP ($\Lambda_{\mathrm{int}} = v_g\tau_{\mathrm{int}}$) to ensure that there is no more than one intrinsic scattering in a cell. The film boundaries along the y axis behave as black walls with prescribed temperatures, respectively, T_0 and T_ℓ; therefore, they can emit phonons and absorb all incident ones. The phonon flux emitted from each black wall Q^+ is divided into very large number of phonon samples. Note that Q^+ from wall i is connected to the wall temperature T_i through Eq. (43) [19]:

$$Q_i^+ = \frac{S}{4} \sum_{j=L,T,T} \sum_{k=1}^{K_j} \frac{v_{gj}(\omega_k)\hbar\omega_k D_j(\omega_k)}{\exp(\hbar\omega_k/k_B T_i) - 1} \Delta\omega \qquad i = 0, \ell \tag{43}$$

$v_{gj}(\omega_k)$ is the phonon group velocity at frequency band ω_k and polarization mode j. In the MC technique, a large number of frequency bands is required. As in the current DOM, $K_L = 500$ and $K_T = K_L\omega_{m,T}/\omega_{m,L}$ are appropriate.

1.3.2.1. Algorithm. The steady-state MC algorithm is performed as briefly described hereafter:

($s1$) For each phonon sample is assigned a random position on the boundary area, a random direction in the inward hemispherical space, a random frequency and a random polarization mode. Then, the method consists of tracking one by one the phonon samples emitted from the two emitting boundaries. The phonon moves according to a drift motion while its direction is altered when it interacts with material imperfection such as *defect*, *impurity*, or it is reflected by a boundary. The track of phonon is stopped when it is absorbed at an absorbing element (boundary or cell). Each time a phonon is absorbed, the energy of the absorbing element is incremented by the phonon energy. After tracking all samples emitted from boundaries, the energy absorbed (per unit time) at each element, denoted by Q^- for the boundaries and G^- for the

cells, is computed. The superscript "–" indicates that the phonons are absorbed at the element.

($s2$) From each cell, a certain number of phonons are emitted so that the cell emitted-energy, denoted by G^+, is equal to the cell absorbed-energy (energy conservation). Note that during the emission process, new (i.e. different from that of absorbed-phonons) wave vector directions, frequencies, and polarizations are randomly attributed to the emitted phonons. In this manner, the transition of frequency and polarization branches during three-phonon processes is accounted for. These newly emitted phonons are tracked again one by one until they are all absorbed according to the reasons mentioned in step ($s1$). After this phonon tracking, the energies absorbed at cells and walls only during this step, hereafter referred to as "energies absorbed step by step" are computed.

($s3$) While the energies absorbed step by step at cells and walls are greater than zero, they are added to the absorbed-energies (G^- for walls and Q^- for cells) and the algorithm goes back to step ($s2$). Since the phonons absorbed at boundaries are not reintroduced, the total phonon number in the studied system decreases step by step and becomes equal to zero after a certain number of steps. In term of energy, the energies absorbed step by step at cells and walls change with the simulation step and decrease up to zero after a certain number of steps.

The necessary information can be extracted from the simulation statistics. For example, the equivalent temperature of cell i, i.e. T_i, is extracted from G_i^- ($\approx G_i^+$ at steady-state regime) through Eq. (44) while the net energy flux crossing the boundary Q is obtained from the absolute difference between Q^- and Q^+.

$$G_i^- \approx V_i \sum_{j=L,T,T} \sum_{k=1}^{K_p} \left[\frac{\tau_{3ph,j}^{-1}(\omega_k, T_i) D_j(\omega k) \hbar \omega_k}{\exp(\hbar\omega_k / k_B T_i) - 1} \right] \Delta\omega \quad i = 1, Ncell \qquad (44)$$

where V_i is the volume of the cell i. $\tau_{3ph,j}^{-1}(\omega_k, T_i)$ is the frequency-, polarization-, and temperature-dependent relaxation rate, defined in Eqs. (17)–(20).

As the initial cell temperatures are unknown, the frequency distribution of phonons in the cells is not correct. Therefore, iteration on the temperatures is required until the temperature profile is unchanged. This consists of repeating the steps ($s1$) to ($s3$) using as initial temperatures the latest computed temperatures. These different simulation steps are well detailed in our recent paper [19].

For various test cases, it is shown that only 2 or 3 temperature iterations are required to reach the convergence [19]. Once the simulation convergence is achieved, the out-of-plane thermal conductivity, k_{out}, can be deduced from Eq. (42) using $q = Q/S$ as net flux per unit surface.

The left ($y = 0$) and right ends ($y = l$) of the simulation box are totally absorbing walls; therefore, each incident phonon is absorbed and the track of its path is stopped. The remaining boundaries are specular reflecting walls that enable to mimic the one-dimensional heat transfer condition. Therefore, each incident phonon is reflected into the specular direction then its path continues without energy alteration.

1.4. Results

In this work, we use Eqs. (21) and (28) to calculate the in-plane thermal conductivity of silicon thin films (using the height to width ratio condition $h/w = 100$) and silicon nanowires (considering square wire cross-section $h/w = 1$). Instead of fixing the value of the specular probability parameter p commonly used in literature, its value is evaluated from Eqs. (30) and (31) considering $\eta = 1.5a$ for all silicon nanostructures. This value of $\eta = 1.5a$ is fitted from experimental measurement of thermal conductivity of nanostructures. This parameter η corresponds to the roughness of boundaries. For silicon thin films, the current theoretical results are compared with experimental data of Asheghi and co-workers [7] while for silicon nanowires, comparison of the current proposed model with measurements of Li et al. [8] is performed. Also, the results considering totally diffuse boundary scattering (i.e. $p = 0$), the BZBC dispersion and the corresponding relaxation times are shown. For thin films, results for thicknesses w equal to 20 nm, 100 nm, and 420 nm over the temperature range 20–1000 K are shown in Fig. 5. For nanowires, results for different widths w equal to 22 nm, 37 nm and 115 nm and temperatures in the range 20–1000 K are depicted in Figs. 6 and 7. It can be noted that:

(i) At low temperatures ($T < 30$ K) where low frequency phonons dominate the energy transport, the effect of dispersion approximation is negligible because both models of dispersion are globally similar. Moreover, the current calculation of in-plane thermal conductivities of thin films and nanowires agree well with experimental data. This tends to confirm that the proposed boundary scattering model using frequency dependent specular probability parameter is appropriate.

(ii) At high temperatures ($T > 30$ K), the influence of dispersion model is more noticeable. The in-plane thermal conductivity calculated using Holland dispersion is systematically greater than that obtained using the BZBC dispersion model. The largest deviation (about 75%) is observed in the case of thinnest nanostructures at 1000 K. The deviation between calculations using Holland and BZBC dispersion can be explained by the fact that at higher temperatures, high frequencies play an important role in the energy transport and in this frequency range, the dissimilarity between the Holland and BZBC dispersion approximations is more significant. Due to boundary scattering, the intrinsic MFP using BZBC dispersion is much reduced than that using the Holland dispersion. As result, the calculated in-plane thermal conductivity using the BZBC dispersion is smaller than that calculated using the Holland dispersion. i.e.: $k_{in,H} > k_{in,B}$.

(iii) Except for the case of nanowire of size 22 nm (Fig. 7), globally good agreement is observed between the experimental in-plane thermal conductivity and that predicted using the BZBC dispersion model. That tends to show that the BZBC dispersion model is appropriate to predict in-plane thermal

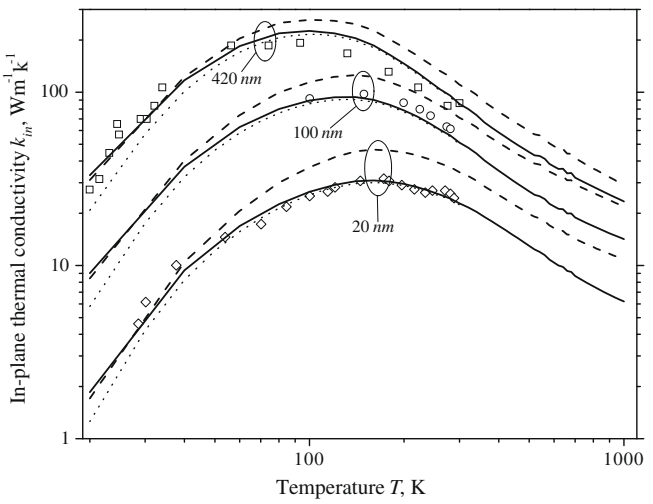

Fig. 5. Temperature dependent in-plane thermal conductivity of silicon thin films of different thicknesses. Open symbols: experimental data from [7]; Dot lines: current prediction using BZBC model using $p = 0$; solid lines: current prediction using BZBC model using variable p; dash lines: current prediction using Holland dispersion model using variable p.

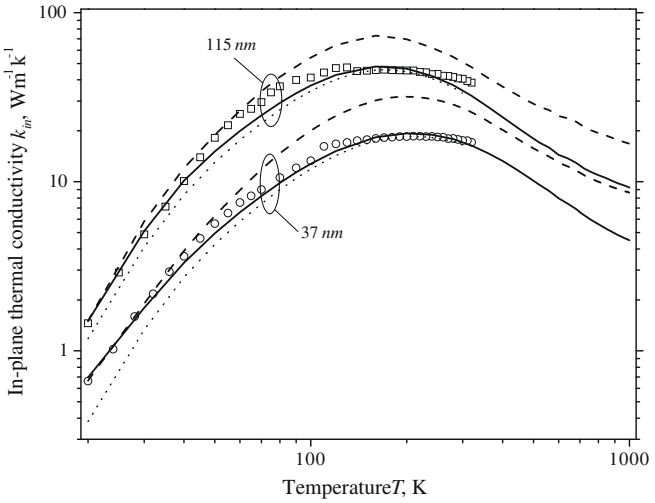

Fig. 6. Temperature dependent in-plane thermal conductivity of silicon nanowires of widths 37 nm and 115 nm. Open symbols: experimental data from [8]; dot lines: current prediction using BZBC model using $p = 0$; solid lines: current prediction using BZBC model using variable p; dash lines: current prediction using Holland dispersion model using variable p.

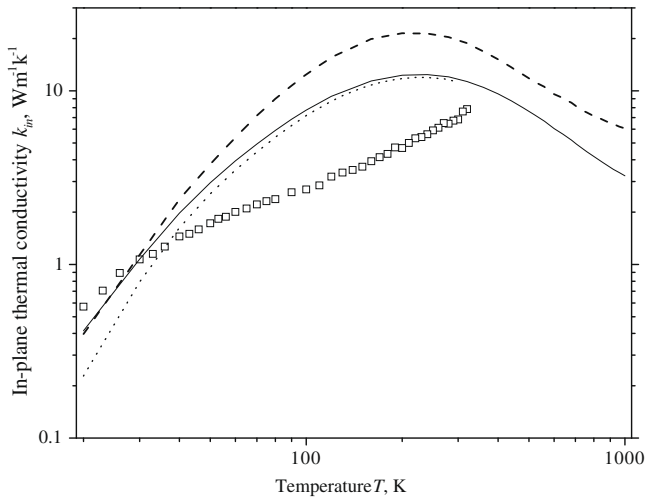

Fig. 7. Temperature dependent in-plane thermal conductivity of silicon nanowires of width 22 nm. Open symbols: experimental data from [8]; dot lines: current prediction using BZBC model using $p = 0$; solid line: current prediction using BZBC model using variable p; dash line: current prediction using Holland dispersion model using variable p.

conductivity of nanostructures. In fact, for these nanostructures, the phonon confinement is not significant, i.e. the phonon dispersion curves are well described using the BZBC model. The deviation of calculations from experimental data in the case of very thin wire (width of 22 nm) is observed. The presence of high density of impurities not accounted for in the models may cause this deviation but not sufficient to explain it. Recall that previous works have evoked the confinement effect that tends to decrease the thermal conductivity beyond the boundary scattering effect [17].

(iv) The predictions at low temperatures using frequency dependent specular probability parameter are globally in better agreement with low temperature experimental data than calculations considering identical dispersion model (BZBC) and relaxation times and totally diffuse scattering ($p = 0$). Previous works on out-of-plane thermal conductivity have been made in the past but they are mainly focused on thick samples where the transport regime is in the diffusion limit, hence, the size effect (boundary scattering) and end effect (temperature shifts at boundaries) becomes mute. Excepted for low temperature ($0.1\ K \leqslant T \leqslant 100\ K$) measurements of thermal conductivity across silicon samples of centimeter sizes carried out by Klitsner et al. [39], to our knowledge, there are no experimental data of out-of-plane thermal conductivity of thin film to compare with our results. Recent molecular dynamics data [4,5] may be taken as reference but they have been mainly focuses on very thin silicon films (thickness about 10 of nanometers) [4] where the validity of Boltzmann transport equation may be questionable due to wave effect. Therefore, in this study, we focus our attention on quantitative comparison between the MC simulation and DOM.

A series of simulations is performed for several silicon film thickness 20 nm, 100 nm, and 0.42 μm at different temperatures from 150 K to 1000 K. Note that, for temperatures less than 150 K, the phonon transport is mainly ballistic for film thickness less than several micrometers (cf. Fig. 4 for 100 μm thick silicon film); therefore, the temperature of the entire film is nearly constant with discontinuities at the two boundaries. In these cases the concept of conductivity is questionable. Thicker films are not investigated because the dispersion effect disappears in these cases. Moreover, MC simulations are only carried out for temperatures up to 500 K due to excessive computation time for high temperature simulations. In DOM and MC calculations, the difference in temperature between the two boundaries of the film is always maintained at 20 K and it is assumed that the computed thermal conductivity from the simulation is the representative thermal conductivity at the average temperature of the film. To point out the anisotropy of thermal conductivity, the out-of-plane thermal conductivity is compared for the same silicon film thicknesses with the in-plane thermal conductivity experimentally measured (for temperatures less than 300 K) [7] and that predicted just above using the BZBC dispersion (for temperatures greater than 300 K). According to Fig. 8 in which comparison of results is reported, we can see that:

(i) The solution of the BTE for phonons using DOM and the MC simulation give globally identical results. At temperatures lower than 200 K more significant deviation between DOM and MC results is noted. This deviation can be attributed to the difficulty in evaluating the temperature gradient in the film. In fact, when the temperature gradient within the film is small, a small error in the temperature gradient induces high deviation on thermal conductivity. The slight deviation of the DOM solutions from the MC results at higher temperature may be attributed to the omission of transition between polarization modes during three-phonon scattering in the DOM. According to previous work of Mazumder and Majumdar [16], the probability of transition of longitudinal mode to transverse one increases with temperature; hence, it may affect the thermal conductivity at higher temperature.

(ii) When film thickness decreases and/or the temperature increases, the influence of the phonon dispersion approximation becomes more noticeable. The results obtained using Holland dispersion are greater than that obtained from the BZBC dispersion. The reason of this deviation can be explained in the same manner as for the case of in-plane thermal conductivity because we can always use the concept of reduction of intrinsic MFP due to boundary scattering.

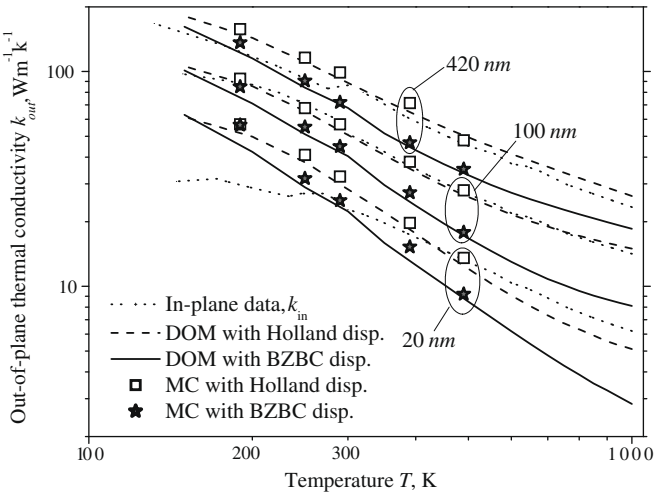

Fig. 8. Temperature dependent out-of-plane thermal conductivity of silicon films of thicknesses 20 nm, 100 nm, and 420 nm. Square symbols: MC simulation using Holland dispersion model; star symbols: MC simulation using BZBC dispersion model; solid lines: DOM result using BZBC model; dash lines: DOM result using Holland dispersion model. Dot lines: experimental data ($T \leqslant 300$ K) [7] and theoretical calculation based on BZBC dispersion ($T > 300$ K) of in-plane thermal conductivity.

(iii) Both in-plane and out-of-plane thermal conductivities of the studied films have the same order of magnitude in the considered temperature range except for the case of 20 nm thick film and temperature lower than 200 K. For films of thicknesses 100 nm and 420 nm, k_{in} is greater than k_{out} and they converge to the same value at 150 K. At high temperature ($T > 300$ K), k_{out} is systematically smaller than k_{in} because the phonon mean free path in the out-of-plane direction is much shorter than that in the in-plane direction. In fact, boundaries of films in the case of out-of-plane phonon transport are totally absorbing, therefore they absorb all incident phonons while the boundaries in the case of in-plane phonon transport are totally diffuse reflecting. For temperature lower than 100–200 K and films of thickness 20 nm, k_{in} decreases with temperature (as it is shown in Fig. 5) while k_{out} increases with temperature. This behavior of k_{out} is due to the ballistic effect (i.e., there is temperature shifts at boundaries and the temperature gradient decreases as the temperature decreases).

This comparison between the in-plane and out-of-plane thermal conductivities tends to show that there is anisotropy of thermal conductivity of silicon films and it is particularly pronounced at low temperatures and thinner films as it is expected.

2. Conclusion

Although the bulk thermal conductivity has been successfully predicted using different approximations of phonon dispersion, e.g. the famous Debye, Callaway, and Holland dispersion models, there is lack of knowledge concerning their validity on the thermal conductivity calculation of nanostructures. One of the originality of this current work is the investigation of the influence of phonon dispersion approximation on both in-plane and out-of-plane thermal conductivities of nanostructures. The usual Holland dispersion approximation and a more refined, straightforward, dispersion model known Brillouin zone boundary condition (BZBC) model are analyzed. The relaxation times are modeled by the formulations suggested by Holland. For the BZBC dispersion, new relaxation time parameters fitted from bulk thermal conductivity data are reported. Calculations of in-plane thermal conductivity of silicon thin films and nanowires of different sizes, over large temperature interval are compared with experimental data and simulation results reported in literature. Due to lack of experimental and theoretical data of out-of-plane thermal conductivity, the Discrete ordinate method (DOM) and the Monte Carlo (MC) simulation are compared considering silicon thin films of different thicknesses at different temperature levels. The conclusions are the following:

(i) The influence of phonon dispersion approximation is significant in both in-plane and out-of-plane thermal conductivity of silicon thin films and silicon nanowires, especially for ultra thin nanostructures and/or at high temperatures. In these cases, calculations based on Holland dispersion approximation overestimate thermal conductivity of nanostructures due to drastic simplification of dispersion curves. This confirms the previous conclusion of Mingo et al. [21] in the case of nanowires. In the other hand, more refined dispersion model (compared to experimental data) such as the BZBC dispersion is shown to be well adequate for calculation of in-plane thermal conductivity of silicon thin films and nanowires with characteristic sizes greater than 20–30 nm. Since, calculations based on BZBC dispersion involve no fitting to any nanostructure measurements, they are thus fully predictive approaches. The only fitting is the relaxation time parameters involving only the bulk thermal conductivity measurements. Moreover, these new relaxation time parameters are very useful for other powerful techniques such as the solution of the Boltzmann transport equation.

(ii) The in-plane thermal conductivity model developed in this study enables to calculate satisfactorily the thermal conductivity along silicon thin films and silicon nanowires without recourse to more complex and time consuming methods such as DOM, MC and molecular dynamics simulations.

(iii) The out-of-plane thermal conductivities are pseudo conductivities, depending on thickness. They are calculated using the current DOM and MC simulation. Both prediction methods are globally in good agreement.

(iv) Finally, the anisotropy of thermal conductivity of silicon thin films, i.e. the contrast between the in-plane and out-of-plane thermal conductivity, is pointed out and shown to be significant at low temperatures and very thin films.

Appendix A. Explicit forms of F_{min} and F_{max} according to reference [28]

$$F_{\min}^{-1} = \frac{3}{\pi w h}\int_0^w dy \int_0^h dx \sum_{i=1}^{6} \int_{\phi_{i-1}}^{\phi_i} d\phi \int_0^{\pi/2} \times d\theta \sin\theta \cos^2\theta \left\{1 - (1-p)e^{-d_{1,i}^*} - p(1-p)e^{-(d_{1,i}^* + d_{2,i}^*)}\right\} \tag{A.1}$$

and

$$F_{\max}^{-1} = \frac{3}{\pi w h}\int_0^w dy \int_0^h dx \sum_{i=1}^{6} \times \int_{\phi_{i-1}}^{\phi_i} d\phi \int_0^{\pi/2} d\theta \sin\theta \cos^2\theta \left\{1 - (1-p)e^{-d_{1,i}^*} - pe^{-(d_{1,i}^* + d_{2,i}^*)}\right\} \tag{A.2}$$

with $d_{1,i}^* = L_{1,i}/\Lambda_{\text{int}}$ and $d_{2,i}^* = L_{2,i}/\Lambda_{\text{int}}$

The definition of $L_{1,i}$, $L_{2,i}$ and φ_i for $i = 1$ to 6 are:

$$L_{1,i} = \frac{L_{\perp}^{1,i}}{\sin\theta},$$
$$L_{2,i} = \frac{L_{\perp}^{2,i}}{\sin\theta},$$
$$L_{\perp}^{1,1} = L_{\perp}^{1,2} = L_{\perp}^{1,3} = \frac{h-y}{\sin\phi},$$
$$L_{\perp}^{1,4} = L_{\perp}^{1,5} = L_{\perp}^{1,6} = \frac{-x}{\cos\phi},$$
$$L_{\perp}^{2,1} = \frac{w-x}{\cos\phi} - \frac{h-y}{\sin\phi},$$
$$L_{\perp}^{2,2} = \frac{h}{\sin\phi},$$
$$L_{\perp}^{2,3} = \frac{-x}{\cos\phi} - \frac{h-y}{\sin\phi},$$
$$L_{\perp}^{2,4} = \frac{h-y}{\cos(\phi-\pi/2)} - \frac{x}{\sin(\phi-\pi/2)},$$
$$L_{\perp}^{2,5} = \frac{w}{\sin(\phi-\pi/2)},$$
$$L_{\perp}^{2,6} = \frac{y}{\sin(\phi-\pi)} - \frac{x}{\cos(\phi-\pi)},$$
$$\phi_0 = \arctan\left(\frac{h-y}{w-x}\right),$$
$$\phi_1 = \arctan\left(\frac{2h-y}{w-x}\right),$$
$$\phi_2 = \frac{\pi}{2} + \arctan\left(\frac{x}{2h-y}\right),$$
$$\phi_3 = \frac{\pi}{2} + \arctan\left(\frac{x}{h-y}\right),$$
$$\phi_4 = \frac{\pi}{2} + \arctan\left(\frac{w+x}{h-y}\right),$$
$$\phi_5 = \pi + \arctan\left(\frac{y}{w+x}\right),$$
$$\phi_6 = \pi + \arctan\left(\frac{y}{x}\right).$$

References

[1] A. Majumdar, Microscale heat conduction in dielectric thin films, J. Heat Transfer 115 (1993) 7–16.
[2] S. Volz, G. Chen, Molecular dynamics simulation of thermal conductivity of silicon nanowires, Appl. Phys. Lett. 75 (14) (1999) 2056–2058.
[3] J.R. Lukes, D.Y. Li, X.G. Liang, C.L. Tien, Molecular dynamics study of solid thin-film thermal conductivity, J. Heat Transfer 122 (2000) 536–543.
[4] Xi-Li Feng, Z.-X. Li, Z.-Y. Guo, Molecular dynamic simulation of thermal conductivity of nanoscale thin silicon films, Microsc. Thermophys. Eng. 7 (2003) 153–161.
[5] C.J. Gomes, M. Madrid, J.V. Goicochea, C.H. Amon, In-plane and out-of-plane thermal conductivity of silicon thin films predicted by molecular dynamics, J. Heat Transfer 128 (2006) 1114–1122.
[6] M. Asheghi, M.N. Touzelbaev, K.E. Goodson, Y.K. Leung, S.S. Wong, Temperature-dependent thermal conductivity of single-crystal silicon layers in SOI substrates, J. Heat Transfer 120 (1998) 31–36.
[7] W. Liu, M. Asheghi, Thermal conductivity measurements of ultra-thin single crystal silicon layers, J. Heat Transfer 128 (1) (2006) 75–83.
[8] D. Li, Y. Wu, P. Kim, L. Shi, P. Yang, A. Majumdar, Thermal conductivity of individual silicon nanowires, Appl. Phys. Lett. 83 (2003) 2934–2936.
[9] M.G. Holland, Analysis of lattice thermal conductivity, Phys. Rev. 132 (1963) 2461–2471.
[10] P. Chantrenne, J.L. Barrat, X. Blasé, J.D. Gale, An analytical model for the thermal conductivity of silicon nanostructures, J. Appl. Phys. 97 (2005) 104318.
[11] J. Zou, A. Balandin, Phonon heat conduction in a semiconductor nanowire, J. Appl. Phys. 89 (2001) 2932–2938.
[12] M.-J. Huang, W.-Y. Chong, T.-M. Chang, The lattice thermal conductivity of a semiconductor nanowire, J. Appl. Phys. 99 (2006) 114318.
[13] S.V.J. Narumanchi, J.Y. Murthy, C.H. Amon, Submicron heat transport model in silicon accounting for phonon dispersion and polarization, J. Heat Transfer 126 (6) (2004) 946–955.
[14] S. Volz, D. Lemonnier, J.B. Saulnier, Clamped nanowire thermal conductivity based on phonon transport equation, Microsc. Thermophys. Eng. 5 (3) (2001) 191–207.
[15] R.A. Escobar, B. Smith, C.H. Amon, Lattice Boltzmann modeling of subcontinuum energy transport in crystalline and amorphous microelectronic devices, J. Elect. Pack. 128 (2) (2004) 115–124.
[16] S. Mazumder, A. Majumdar, Monte Carlo study of phonon transport in solid thin films including dispersion and polarization, J. Heat Transfer 123 (2001) 749–759.
[17] Y. Chen, D. Li, J.R. Lukes, A. Majumdar, Monte Carlo simulation of silicon nanowire thermal conductivity, J. Heat Transfer 127 (2005) 1129–1137.
[18] D. Lacroix, K. Joulain, D. Lemonnier, Monte Carlo transient phonon transport in silicon and germanium at nanoscales, Phys. Rev. B 72 (2005) 064305.
[19] J. Randrianalisoa, D. Baillis, Monte Carlo simulation of steady-state microscale phonon transport, J. Heat Transfer, 130 (2008) 072404.
[20] J.D. Chung, A.J.H. Mc Gaughey, M. Kaviany, Role of phonon dispersion in lattice thermal conductivity modeling, J. Heat Transfer 126 (2004) 376–380.
[21] N. Mingo, Calculation of Si nanowire thermal conductivity using complete phonon dispersion relations, Phys. Rev. B 68 (2003) 113308.
[22] C. Kittel, Introduction to Solid State Physics, sixth ed., Willey, New York, 1986.
[23] B.N. Brockhouse, Lattice vibrations in silicon and germanium, Phys. Rev. Lett. 2 (1959) 256–258.
[24] J.M. Ziman, Electrons and Phonons, second ed., Cambridge University Press, London, 2001.
[25] D.J. Ecsedy, P.G. Klemens, Thermal resistivity of dielectric crystals due to four-phonon processes and optical modes, Phys. Rev. B 15 (1993) 5957–5962.
[26] S. Tamura, H.J. Maris, Temperature dependence of phonon lifetime in dielectric crystal, Phys. Rev. B 51 (1995) 2857–2863.
[27] E.H. Sondheimer, The mean free path of electrons in metals, Adv. Phys. 50 (6) (2001) 499–537.
[28] D. Josell, C. Burkhard, Y. Li, Y.-W. Cheng, R.R. Keller, C.A. Witt, D.R. Kelley, J.E. Bonevich, B.C. Baker, T.P. Moffat, J. Appl. Phys. 96 (2004) 759–768.
[29] P. Beckmann, A. Spizzichino, The Scattering of Electromagnetic Waves from Rough Surfaces, Oxford Pergamon Press, London, 1963.
[30] M.Q. Brewster, Thermal Radiative Transfer and Properties, Wiley, New York, 1992.
[31] G. Chen, C.L. Tien, Thermal conductivities of quantum well structures, J. Thermophys. Heat Transfer 7 (2) (1993) 311–318.
[32] K.E. Goodson, Thermal conduction in nonhomogeneous CVD diamond layers in electronic microstructures, J. Heat Transfer 118 (1996) 279–286.
[33] G. Chen, Thermal conductivity and ballistic phonon transport in the cross-plane direction of superlattices, Phys. Rev. B 57 (1998) 14958–14973.
[34] L. Pilon, K.M. Katika, Modified method of characteristics for simulating microscale energy transport, J. Heat Transfer 126 (2004) 735–743.
[35] R. Prasher, Photon transport in anisotropic scattering particulate media, J. Heat Transfer 125 (2003) 1156–1162.
[36] B.G. Carlson, K.D. Lathrop, Transport theory: the method of discrete ordinates, in: Computing Methods in Reactor Physics, Gordon and Breach, New York, 1968, pp. 167–265.
[37] W.A. Fiveland, Discrete-ordinates solution of the radiative transport equation for rectangular enclosures, J. Heat Transfer 106 (1984) 699–706.
[38] D. Baillis, J.F. Sacadura, Directional spectral emittance of a packed bed: influence of the temperature gradient in the medium, J. Heat Transfer 124 (5) (2002) 904–911.
[39] T. Klitsner, J.E. VanCleve, H.E. Fischer, R.O. Pohl, Phonon radiative he at transfer and surface scattering, Phys. Rev. B 38 (1988) 7576–7594.